Nat. Hazards Earth Syst. Sci. Discuss., 1, 5057–5086, 2013
www.nat-hazards-earth-syst-sci-discuss.net/1/5057/2013/
doi:10.5194/nhessd-1-5057-2013

Natural Hazards and Earth System Sciences
Discussions

Seasonal predictability of the 2010 Russian heat wave

P. Katsafados[1], **A. Papadopoulos**[2], **G. Varlas**[1,2], **E. Papadopoulou**[1], **and E. Mavromatidis**[1]

[1]Department of Geography, Harokopion University of Athens, 70 El. Venizelou Str., Athens, 17671, Greece
[2]Institute of Marine Biological Resources and Inland Waters, Hellenic Centre for Marine Research, Anavyssos, Attiki, Greece

Received: 29 August 2013 – Accepted: 6 September 2013 – Published: 26 September 2013

Correspondence to: P. Katsafados (pkatsaf@hua.gr)

Published by Copernicus Publications on behalf of the European Geosciences Union.

Abstract

The prevailed atmospheric blocking over Eastern Europe and Western Russia during July and August 2010 led in the development of the devastating Russian heat wave. Therefore the question whether the event was predictable or not is highly important. The principal aim of this study is to examine the predictability of this high-impact atmospheric event on a seasonal time scale. To this end, a set of dynamical seasonal simulations have been carried out using an Atmospheric Global Circulation Model (AGCM). The impact of various model initializations on the predictability of this large scale event and its sensitivity to the initial conditions has been also investigated. Ensemble seasonal simulations indicated that only a few individual members reproduced the main features of the blocking system 3 months ahead. Most members missed the phase space and the velocity of the system setting limitations in the predictability of the event.

1 Introduction

During the second half of July and beginning of August 2010, Eastern Europe and Western Russia experienced a strong heat wave resulting in over 55 000 deaths. The wildfires in Russia amplified the impacts of the drought in the area and led in significant decrease of the annual crop production by 25 % and a total loss to the local economy of more than 15 billion US dollars (Barriopedro et al., 2011). This heat wave was more intense compared to temperature reconstructions from the last half millennia (Sedláček et al., 2011) and covered a wider area than the heat wave over Europe during the summer of 2003 (Stott et al., 2004; Schär and Jendritzky, 2004). According to Barriopedro et al. (2011), such kind of mega-heat waves are more likely to break the 500-yr-long seasonal temperature records over approximately 50 % of Europe. According to regional multi-model experiments, the probability of a summer experiencing mega-heat waves is expected to increase by a factor of 5 to 10 within the next 40 yr. However, the magnitude of the 2010 event was so extreme that despite this prediction, the likelihood

of an occurrence of a comparable event over the same region remains fairly low until the second half of the 21st century.

The Euro-Russian heat wave resulted from a strong blocking anticyclone that persisted over Eastern Europe driving warm air from Africa and Arabic peninsula to Western Russia and leading to unprecedented temperatures. During the blocking period the orientation of the anticyclone favored a cold northerly airflow towards the Indian Ocean which interacted with low-level warm and humid air and initiated the heavy rainfall across the Gangetic Plains between the Bay of Bengal in the east to northern Pakistan in the west (Webster et al., 2011). The intensity of this event is confirmed by the amount of precipitation received in a single day which exceeded half of the annual rainfall (Ghelli et al., 2010).

Analysis of model simulations indicated that neither anthropogenic influences nor other slowly varying ocean boundary conditions substantially contributed to the magnitude of the event. Rather, a primarily natural effect seems to have triggered the Russian heat wave. The event was mainly attributed to internal atmospheric dynamical processes that produced and maintained an intense and long-lived blocking event. However the intensity of the heat wave was further increased by regional land surface feedbacks (Dole et al., 2011). A possible scenario of positive feedback involves carbon products and particulate matter primarily emitted from the Russian forest fires that would further heat the troposphere and evaporate cloud droplets. This process dynamically affects the atmospheric stability amplifying the heat wave and strengthening the downstream Rossby wave from the large-scale blocking system and finally provoking the Pakistan floods (Lau and Kim, 2012). Similar surface feedbacks and in situ processes were also affected the predictability of the European heat wave in summer 2003 (Weisheimer et al., 2011).

For such intrinsically low-probability with long return period events the questions of whether the event could be predictable and over what lead time are of highly importance. The principal aim of this study is to examine the predictability of the Russian heat wave on a seasonal time scale. Seasonal prediction's significance lies on its abil-

ity to provide early warnings about oncoming and extreme weather episodes that may grow human fatalities and significantly affect the infrastructure and the environment. Forecasts on seasonal to intra-annual time scales rely on comprehensive Atmospheric Global Circulation Models (AGCMs) usually coupled with land surface and hydrodynamic circulation models with an improved understanding among the coupling systems (Gneiting and Raftery, 2005). So, it is of great interest AGCMs to be able to resolve the main atmospheric mechanisms that trigger potential intense phenomena on various spatiotemporal scales and finally to produce credible forecasts. In this study the dynamical seasonal simulations have been carried out using the Community Atmosphere Model (CAM version 3) of the National Center for Atmospheric Research (NCAR). The impact of various model initializations on the predictability of this large scale event has been also investigated, because such comprehensive prognostic systems are sensitive to the initial conditions. This is due to the fact that the chaotic nature of the atmosphere imposes a finite limit of few weeks to the predictability of the atmospheric conditions. Therefore, an ensemble forecasting method was introduced in the context of numerical weather prediction. Ensemble forecasting is assumed as a feasible method to integrate a deterministic forecast with an estimate of the probability distribution of atmospheric states (Buizza, 1997).

2 Description of the synoptic conditions

The nature of the Russian heat wave and its origins were associated to the upper-level atmospheric circulation. During summer 2010 the typical upper-level atmospheric circulation over Asia was differentiated and the Rossby wave anomalies invoked extreme phenomena. An omega blocking pattern characterized the 500 hPa July 2010 flow (Dole and Gordon, 1983). The blocking anticyclone over Russia was the dominant weather pattern prevailing in Europe from late July to mid-August 2010 while the low frequency subtropical jet meanders around it, increasing the meridional component of the anomalous flow at 500 hPa over East Europe transferring warm air at 850 hPa

(Fig. 1). Moreover a widespread ridge at 500 hPa extended from Middle East to East Europe and contributed to the formation of the omega blocking pattern. The mean sea level pressure increased at the areas under the impact of the ridge and the anticyclone at the north European Russia secluded from the westerly airflow intensifying the omega blocking pattern (Fig. 2). The heat wave was trapped over Russia for about three weeks resulting in increasingly high surface temperatures in the area. Furthermore, the high levels of 1000–500 hPa thickness amplified the warm air mass depth (Fig. 3). This rapid geopotential height rise during the block development is characterized as a synoptic-scale pattern or as an interaction between synoptic and planetary scale process (Lupo and Smith, 1998).

As it was recorded from the meteorological stations in the area, the highest July 2010 surface temperature anomalies occurred near the center of the block (Table 1), where northward displaced subtropical air, descending air motions and reduced cloudiness all contributed to abnormally warm surface temperatures (Ghelli et al., 2010). Severe drought occurred with the Russian heat wave, making it likely that land surface feedbacks amplified the heat wave intensity, as has been observed in prior severe droughts (Fischer et al., 2007). Thus, during night time the cooling of the ground surface was intensifying the temperature inversion, resulting to amplification of the anticyclone. The vertical temperature profile over Moscow revealed an intense inversion layer coexisting with a dry air mass in the lower troposphere (Fig. 4).

To the east of the omega block anomalously cool temperatures occurred in conjunction with an upper level trough and southward advection of polar air (Dole et al., 2011). Also, a subtropical jet streak at the level of 200 hPa intensified the divergence in this level and the convergence at the surface level (Uccellini and Johnson, 1979). The interaction between this upper-level jet streak and diabatic processes initiated heavy rainfalls in a widespread area at northern Pakistan (Fig. 5).

3 Model description and methodology

In this study, the seasonal predictability of the Russian heat wave and the Pakistan floods is investigated using the NCAR Community Atmosphere Model (CAM3) which is the atmospheric component of the Community Climate System Model (CCSM). CAM3 is a global AGCM designed to produce simulations for several different dynamical cores and horizontal resolutions. A detailed description of the physics and dynamics of CAM3 can be found in Collins et al. (2004, 2006b). The standard version, used in this study, has 26 vertical levels and an 85-wave triangular spectral truncation (T85L26). The specific Eulerian truncation corresponds to a zonal resolution of $1.41^{\circ} \times 1.41^{\circ}$. In CAM3, the physics and Eulerian or semi-Lagrangian dynamical cores are process split, while the physics and Finite Volume (FV) core are time split (Williamson, 2002). The diagnostic cloud water scheme used in a previous version of the model has been replaced by the prognostic cloud water parameterization of Rasch and Kristjánsson (1998) updated by Zhang et al. (2003). Concerning the radiative process, the model includes separate evolution equations for the liquid and ice-phase condensate and the revised scheme includes a new formulation of the fractional condensation rate and a self-consistent treatment of the evolution of water vapor, heat, cloud fraction, and in-cloud condensate (Zhang et al., 2003). The aerosol dataset includes the annually cyclic, monthly mean distributions of sulfate, sea salt, carbonaceous, and soil-dust aerosols. The climatology is derived from a chemical transport model constrained by assimilation of satellite retrievals of aerosol depth (Collins et al., 2001). The climatology in CAM3 is obtained from aerosol assimilation for the period 1995–2000. CAM3 also includes the Community Land Model (CLM) for the treatment of land surface energy exchanges. The model examines the physical, chemical, and biological processes by which terrestrial ecosystems affect and are affected by climate across a variety of spatial and temporal scales (Oleson et al., 2004). Stand-alone integrations with CAM3 employ a global Sea Surface Temperature (SST) and Sea-Ice Conditions (SIC) data sets similar to that utilized by the ECMWF (Fiorino, 2004) based on 40-yr reanalysis project (ERA-40).

In this study the performance of the model has been assessed by simulating the large scale blocking system developed over Eastern Europe and Russia in July and August 2010. To this end, seasonal simulations of the CAM3 coupled with the CLM have been carried out using a time-variant climatological SST dataset for the definition of the sea surface boundary condition. The simulations were based on a modified version of the lagged average forecast (LAF) formulation introduced by Hoffman and Kalnay (1983). In a short range forecast the LAF method consists of ensemble members that include the latest operational forecast, and also forecasts for the same verification time started a few days earlier than the latest one (Dalcher et al., 1988). Thus each member includes the governing dynamics and it can be considered as a perturbation about the ensemble mean. In accordance to the LAF methodology, CAM3 seasonal scale simulations were initialized from the daily global analysis assuming each analysis as a perturbation of the previous one due to the long lead time of 2–7 months ahead. Thus, the ensemble consists of 61 members with different initialization dates and different simulation lengths, but with identical end time. In particular, each member was initialized by the Global Forecasting System (GFS) analyses on 00:00 UTC of each day of January and April 2010 and performed a simulation up to September 1st at 00:00 UTC. Hence, the first model run (member) was initialized by the 00:00 UTC, 1 January GFS analysis and performed the simulation for 8 months (243 days). The second run started at 00:00 UTC, 2 January and produced a simulation of 242 days. Likewise, the member 32 was initialized by the 00:00 UTC, 1 April GFS analysis and integrated for a period of 5 months (153 days). Finally, the last ensemble member was initialized by the 00:00 UTC, 30 April 2010 GFS analysis with simulation period of 4 months (124 days).

In this way, 31 members were produced with 5 through 8 months lead time for the period June, July, August (JJA) and 30 members were produced with 2 through 5 months lead time for the same period (Fig. 6). In order to assign the estimated temperature anomaly, monthly averaged model outputs compared against long term monthly means valid for the period of 1971–2000, released by the National Center for Environmental Predictions (NCEP) and NCAR (Kalnay et al., 1996). Moreover, spaghetti plots of the

temperature at 850 hPa have been also produced as a guidance provision of each member uncertainty.

4 Predictability of the atmospheric blocking

4.1 Temperature at 850 hPa and geopotential height at 500 hPa

The simulated temperature at 850 hPa and geopotential height at 500 hPa of individual ensemble members are compared against the relevant ECMWF operational analyses in order to evaluate the predictability of the event. Some members indicate an early warning of the event and reveal the large scale spatiotemporal characteristics of the blocking system prevailed over Russia even 3 months in advance. For instance, the member initialized at 22 April 2010 and referenced as 0422 reproduced the main blocking pattern over Eastern Europe for 16 July at 12:00 UTC (Fig. 7a). However this member simulated a northward extended and more intense system comparing against an early staged blocking system depicted in ECMWF analysis (Fig. 7a). Four days later the 0422 member displaced a mature stage system over central Russia while in ECMWF analysis the blocking pattern was still in developing stages over Eastern Europe (Fig. 8a and b). Despite the fact of the early warning this member missed the phase of the system and its spatiotemporal characteristics as well, predicting a short lived eastward propagating blocking pattern. The individual member initialized at 25 April 2010 and referenced as 0425 further improved the prediction of the blocking system on 16 July at 12:00 UTC (Fig. 9a) reproducing a less northward extended system. However the 0425 displaced the center of the system to the central Russia at 20 July and predicted a short-lived blocking pattern lasted almost 5–6 days (Fig. 9b). This led in overestimation of the temperature advection to the affected area and underestimation of the polar anomaly flow eastward of the blocking system.

4.2 Spaghetti plots of the temperature at 850 hPa

The mean monthly isotherm of the 283 °K obtained from each one of the 61 members is compared against the NCAR/NCEP long-term (based to 1971–2000 period) mean monthly isothermal values of 283 °K (10 °C) and 278 °K (5 °C). This comparison suggests whether the estimated temperatures exceed or not the relevant climatological values for the period under consideration. In Fig. 10a almost all the members that were initialized at January 2010 exceeded the NCEP/NCAR long-term monthly mean temperature at 283 °K for July 2010, predicting increased occurrence probability for higher than normal temperatures over Eastern Europe and Russia. But, only a few members exceeded the long-term isotherm of 278 °K indicating that the predicted temperature anomaly is likely to be less than 5 °K. However, the recorded mean monthly temperature anomalies for July 2010 provided from the National Oceanic and Atmospheric Administration (NOAA) show that the surface temperature anomaly was more than 5 °C over Eastern Europe and Russia (Fig. 12). The spaghetti plots referenced to the mean monthly temperature of August 2010 (Fig. 10b) suggest that almost half of ensemble members exceeded the long-term isotherm of 278 °K. However the divergence of the forecasts within the ensemble indicates that the uncertainty in the forecast can be high. Such reduced predictability is more prominent over the eastern flanks of the blocking system and it is associated with the eastward displacement of the system obtained from almost the entire members initialized in January 2010. The simulations of April 2010 indicate a stronger persistence of higher than normal temperatures over the study area. For July 2010, most of the April members are found in the range of 278 °K and 283 °K long-term means (Fig. 10c) while for August 2010 they are placed northward close to 278 °K (Fig. 10d). For both months the ensemble spread is reduced over Eastern Europe while areas of high uncertainty are located over central Russia. Despite the fact of the long lead period, both January and April members provide similar predictability confidence. Thus, April simulations provide almost negligible predictability improvement comparing against the relevant January simulations. Furthermore, the

comparison between the maximum daily temperatures at 850 hPa obtained from the ensemble members integrated over Eastern Europe and Russia and the corresponding ECMWF analyses did not reveal any strong signal of the extremely hot summer (Fig. 11a and b).

4.3 Temperature anomaly at 850 hPa

Temperature anomaly at 850 hPa is an indication of the model predictability comparing against the NCEP/NCAR long-term monthly means. Figure 13 presents the mean monthly temperature anomaly for August 2010 simulated from the individual member 0422. An extended area over Eastern Europe and Western Russia is characterized by above normal temperatures up to +6 °C and it was combined with negative temperature anomaly eastward of the blocking system driving polar air masses southward and initiating torrential rains in Pakistan. Even though this is an indication of a possible predictability from some individual members almost 4 months in advance, generally this was not the case for most of the ensemble members.

Figure 14 depicts the mean monthly temperature anomalies for July and August 2010 obtained from both forecasting periods, January and April. In Fig. 14a the prevailed temperature anomaly over Russia was up to +2 °C while the maximum anomaly of almost +6 °C was located over the Middle East and the northern areas of Saudi Arabia peninsula. This overestimation of the temperature anomaly over Russia is not considered as a statistically significant in 95 % confidence level. A similar pattern is also clearly depicted in the mean August temperature anomaly obtained from January 2010 ensemble members (Fig. 14b). The comparison against NOAA's mean monthly temperature anomalies (Fig. 12) revealed the model inability to reproduce the local maxima of temperature anomalies. This is a strong indication of reduced predictability of a large-scale event in a lead period of 5–7 months. April members were not able to significantly increase the forecasting skill. Indeed, they simulated secondary maxima of temperature anomaly over Balkan Peninsula and southern Russia (Fig. 14c) and it was combined with a zone of positive anomaly up to +2 °C extended from Eastern Europe

to central Russia in August 2010 (Fig. 14d). Such anomalies include high levels of uncertainty since they are not considered as statistically significant in a 95 % confidence level. The abovementioned analysis confirms that almost the entire members initialized on April 2010 and having 3–5 months lead time did not provide any further predictability improvement. Thus the predictability seems to be independent to the forecast horizon varying from seasonal to intra-annual time scales. This fact is also is in agreement with Matsueda's (2011) statement that the predictability of this particular event has been lost after a few weeks of simulations.

5 Concluding remarks

The predictability of the Russian heat wave on a seasonal time scale has been investigated in this study. The dynamical seasonal simulations have been carried out using the state-of-the-art CAM3 AGCM. The impact of various model initializations on the predictability of the event has been also investigated because such comprehensive prognostic systems are sensitive to the initial conditions due to the chaotic nature of the atmosphere. According to the synoptic analysis, the Russian heat wave provoked by a strong omega blocking system persisted over Eastern Europe and driving warm air from Africa and Arabic peninsula to Western Russia. The vertical temperature profile over Moscow reveals an intense inversion layer coexisting with a dry air mass in the lower troposphere resulting to amplification of the anticyclone. During the blocking period the orientation of the anticyclone favored a cold northerly airflow towards the Indian Ocean which interacts with low-level warm and humid air and triggered heavy rainfall across Northern Pakistan.

Seasonal simulations of the event were based on a modified version of LAF method constructing 61 independent ensemble members initialized on January and April 2010. Each ensemble member has been integrated for 8 and 5 months ahead respectively and in this way, for the period of JJA were produced 31 members on a 5–8 months lead time and 30 members on a 2–5 months lead time.

As far as the predictability is concerned, only a few individual members in April reproduced the main features of the blocking system almost 3 months before the event. For both set of simulations the ensemble spread is relatively limited over Eastern Europe while the areas of high uncertainty are mainly located over central Russia. Most members displaced the basic characteristics of the phase space and the velocity of the system shifting the center eastward and predicting a short-lived blocking pattern. Despite the fact of the long lead period, both January and April members provided similar confidence of the forecast reliability. Thus, almost the entire members initialized on April 2010 and having 2–5 months lead time did not provide any further predictability improvement. Thus the predictability seems to be independent to the forecast horizon varying from seasonal to intra-annual time scales.

The results of this study underline the main difficulties in the seasonal simulation of such high-impact weather event. However, since the LAF method is operationally feasible, due to the fact that the LAF ensemble members can be produced during the normal operational cycle, it is of great importance to investigate furthermore the performance of such ensemble forecasting system. To this end, other recent extreme weather events should be considered.

References

Barriopedro, D., Fischer, E. M., Luterbacher, J., Trigo, R. M., and García-Herrera, R.: The hot summer of 2010: redrawing the temperature record map of Europe, Science, 332, 220–224, doi:10.1126/science.1201224, 2011.

Buizza, R.: Potential Forecast Skill of Ensemble Prediction and Spread and Skill Distributions of the ECMWF Ensemble Prediction System, Mon. Weather Rev., 125, 99–119, doi:10.1175/1520-0493(1997)125<0099:PFSOEP>2.0.CO;2, 1997.

Collins, W. D., Rasch, P. J., Eaton, B. E., Khattatov, B., Lamarque, J. F., and Zender, C. S.: Simulating aerosols using a chemical transport model with assimilation of satellite aerosol retrievals: Methodology for INDOEX, J. Geophys. Res., 106, 7313–7336, 2001.

Collins, W. D., Rasch, P. J., Boville, B. A., Hack, J. J., McCaa, J. R., Williamson, D. L., Kiehl, J. T., Briegleb, B., Bitz, C., Lin, S. J., Zhang, M., and Dai, Y.: Description of the NCAR community atmosphere model (CAM 3.0), Tech. Rep. TN-464+STR NCAR, National Center for Atmospheric Research, Boulder, Colorado, 80307–3000, 226, 2004.

Collins, W. D., Rasch, P. J., Boville, B. A., Hack, J. J., McCaa, J. R., Williamson, D. L., Briegleb, B. P., Bitz, C. M., Lin, S. J., and Zhang, M.: The formulation and atmospheric simulation of the Community Atmosphere Model: CAM3, J. Climate, 19, 2144–2161, 2006.

Fiorino, M.: A multi-decadal daily sea surface temperature and sea ice concentration data set for the ERA-40 reanalysis, ERA-40 Project Report Series No. 12, 16, 2004.

Dalcher, A., Kalnay, E., and Hoffman, R.: Medium-range lagged average forecasts, Mon. Weather Rev., 116, 402–416, 1988.

Dole, R. M. and Gordon, N. D.: Persistent anomalies of the extratropical Northern Hemisphere wintertime circulation: Geographical distribution and regional persistence characteristics, Mon. Weather Rev., 111, 1567–1586, doi:10.1175/1520-0493(1983)111<1567:PAOTEN>2.0.CO;2, 1983.

Dole, R., Hoerling, M., Perlwitz, J., Eischeid, J., Pegion, P., Zhang, T., Quan, X. W., Xu, T., and Murray, D.: Was there a basis for anticipating the 2010 Russian heat wave?, Geophys. Res. Lett., 38, L06702, doi:10.1029/2010GL046582, 2011.

Fischer, E. M., Seneviratne, S. I., Lüthi, D., and Schär, C.: Contribution of land-atmosphere coupling to recent European summer heatwaves, Geophys. Res. Lett., 34, L06707, doi:10.1029/2006GL029068, 2007.

Ghelli, A., Garcia-Mendez, A., Prates, F., and Dahoui, M.: Extreme weather events in summer 2010: how did the ECMWF forecasting systems perform?, ECMWF Newsletter, 125, 7–11, 2010.

Gneiting, T. and Raftery, A. E.: Weather forecasting with ensemble methods, Science, 310, 248–249, doi:10.1126/science.1115255, 2005.

Hoffman, R. N. and Kalnay, E.: Lagged averaged forecasting, an alternative to Monte Carlo forecasting, Tellus, 35A, 100–118, 1983.

Kalnay, E., Kanamitsu, M., Kistler, R., Collins, W., Deaven, D., Gandin, L., Iredell, M., Saha, S., White, G., Woollen, J., Zhu, Y., Chelliah, M., Ebisuzaki, W., Higgins, W., Janowiak, J., Mo, K. C., Ropelewski, C., Wang, J., Leetmaa, A., Reynolds, R., Jenne, R., and Joseph, D.: "The NMC/NCAR 40-Year Reanalysis Project", B. Am. Meteorol. Soc., 77, 437–471, 1996.

Lau, K. M. and Kim, K. M.: The 2012 Russian heat wave/wildfires and Pakistan Flood: Teleconnection of Extremes, J. Hydrometeorol., 13, 392–403, doi:10.1175/JHM-D-11-016.1, 2012.

Lupo, A. and Smith, P. J.: The Interactions between a Midlatitude Blocking Anticyclone and Synoptic-Scale Cyclones that occurred during the Summer Season, Mon. Weather Rev., 126, 502–515, 1998.

Matsueda, M.: Predictability of Euro-Russian blocking in summer of 2010, Geophys. Res. Lett., 38, L06801, doi:10.1029/2010GL046557, 2011.

Oleson, K., Dai, Y., Bonan, G. B., Bosilovichm, M., Dickinson, R., Dirmeyer, P., Hoffman, F., Houser, P., Levis, S., Niu, G. Y., Thornton, P., Vertenstein, M., Yang, Z., and Zeng, X.: Technical description of the Community Land Model (CLM). Technical Report NCAR/TN-461+STR, National Center for Atmospheric Research, Boulder, CO. 80307–3000, 174, doi:10.5065/D6N877R0, 2004.

Rasch, P. J. and Kristjánsson, J. E.: A comparison of the CCM3 model climate using diagnosed and predicted condensate parameterizations, J. Climate, 11, 1587–1614, 1998.

Schär, C. and Jendritzky, G.: Climate change: Hot news from summer 2003, Nature, 432, 559–560, doi:10.1038/432559a, 2004.

Sedláček, J., Martius, O., and Knutti, R.: Influence of subtropical and polar sea-surface temperature anomalies on temperatures in Eurasia, Geophys. Res. Lett., 38, L12803, doi:10.1029/2011GL047764, 2011.

Stott, P. A., Stone, D. A., and Allen, M. R.: Human contribution to the European heatwave of 2003, Nature, 432, 610–614, doi:10.1038/nature03089, 2004.

Uccellini, L. W. and Johnson, D. R.: The Coupling of Upper and Lower Tropospheric Jet Streaks and Implications for the Development of Severe Convective Storms, Mon. Weather Rev., 107, 682–703, 1979.

Webster, P. J., Toma, V. E., and Kim, H. M.: Were the 2010 Pakistan floods predictable?, Geophys. Res. Lett., 38, 40806, doi:10.1029/2010GL046346, 2011.

Weisheimer, A., Doblas-Reyes, F. J., Jung, T., and Palmer, T. N.: On the predictability of the extreme summer 2003 over Europe, Geophys. Res. Lett., 38, L05704, doi:10.1029/2010GL046455, 2011.

Williamson, D. L.: Time-split versus process split coupling of parameterizations and dynamical core, Mon. Weather Rev., 130, 2024–2041, 2002.

Zhang, M., Lin, W., Bretherton, C. B., Hack, J. J., and Rasch, P. J.: A modified formulation of fractional stratiform condensation rate in the NCAR Community Atmosphere Model (CAM2), J. Geophys. Res., 108, 4035, doi:10.1029/2002JD002523, 2003.

Table 1. Maximum near surface temperatures recorded at four meteorological stations in Russia, Belarus and Finland (Source: ECMWF).

Met. Station	Coordinates	Max. Temp. (°C)
Jaskul (Russia)	46.1° N, 45.2° E	42.2 (8/8/2010)
Moscow (Russia)	55.5° N, 37.4° E	39 (30/7/2010)
Gomel (Belarus)	52.2° N, 30.6° E	38.9 (7/8/2010)
Joensuu (Finland)	62.4° N, 29.4° E	37.2 (29/7/2010)

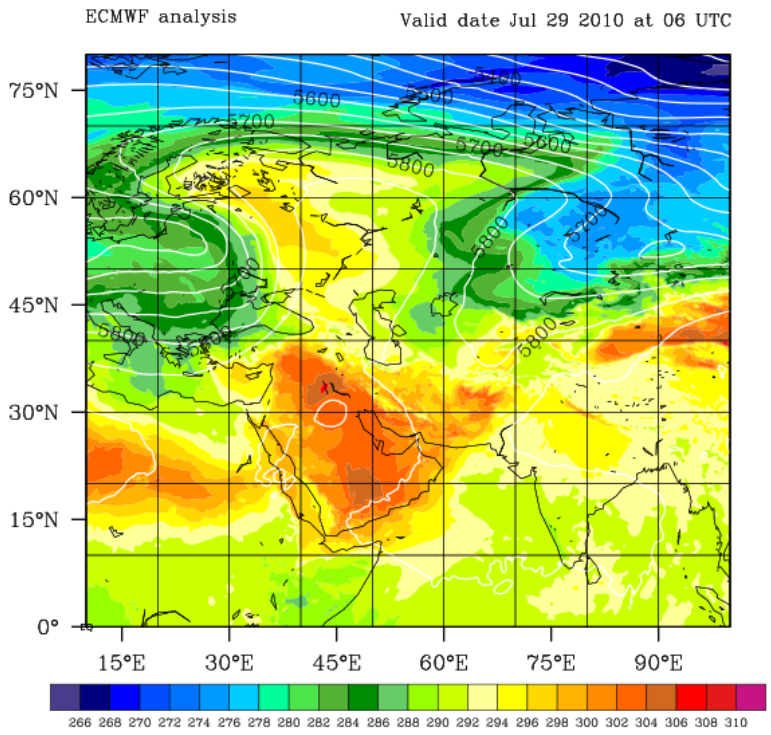

Fig. 1. Temperature at 850 hPa (°K) and geopotential height at 500 hPa (gpm) for 29 July at 06:00 UTC. Data is based on ECMWF operational analysis.

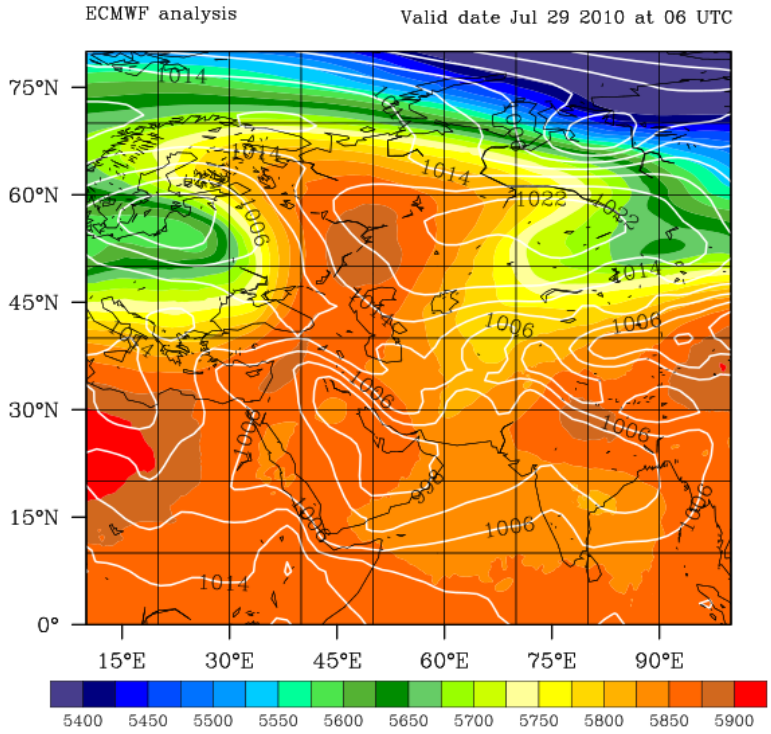

Fig. 2. Mean sea level pressure (hPa) and geopotential height at 500 hPa (gpm) for 29 July at 12:00 UTC. Data is based on ECMWF operational analysis.

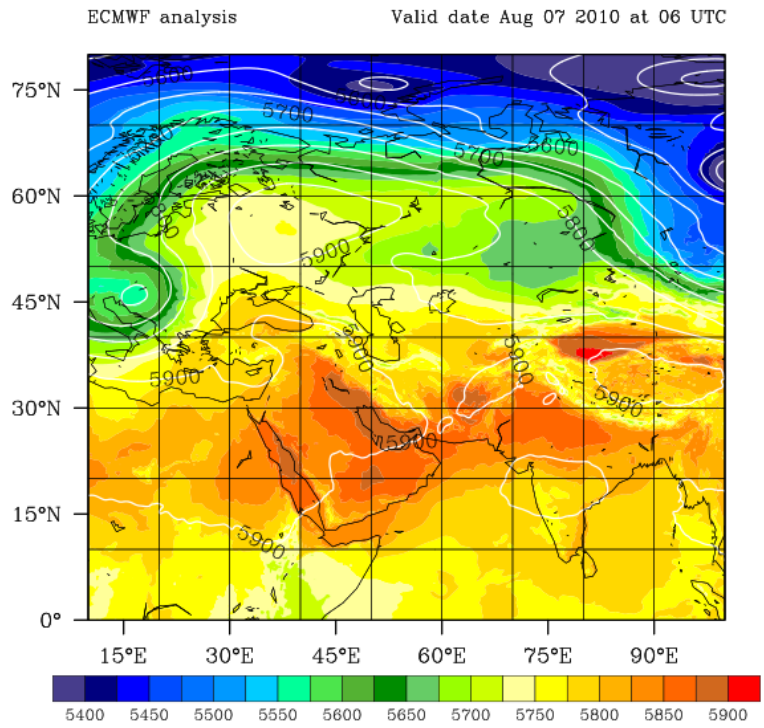

Fig. 3. 1000–500 hPa thickness (gpm) and geopotential height at 500 hPa (gpm) for 7 August at 06:00 UTC. Data is based on ECMWF operational analysis.

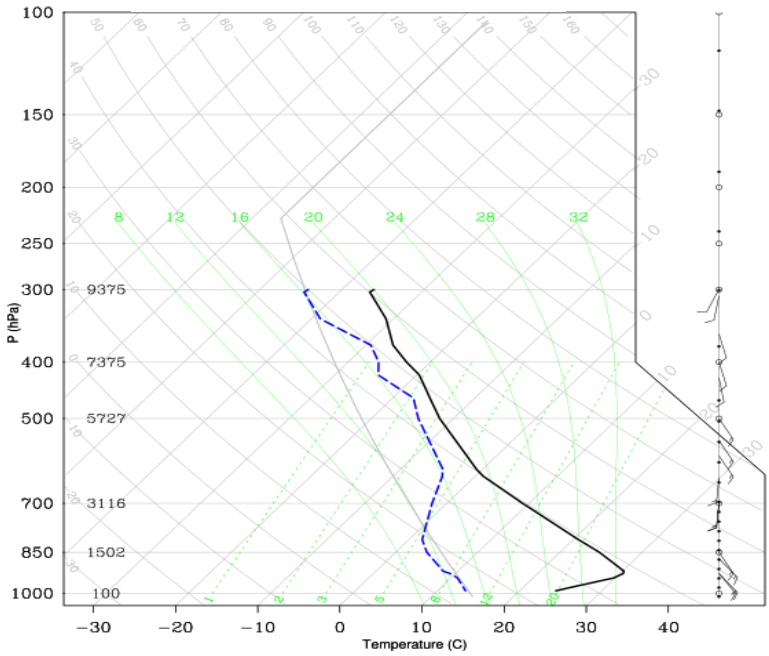

Fig. 4. Skew-T diagrams at Moscow (27612) for 29 July at 00:00 UTC. Radiosonde data is provided by ECMWF.

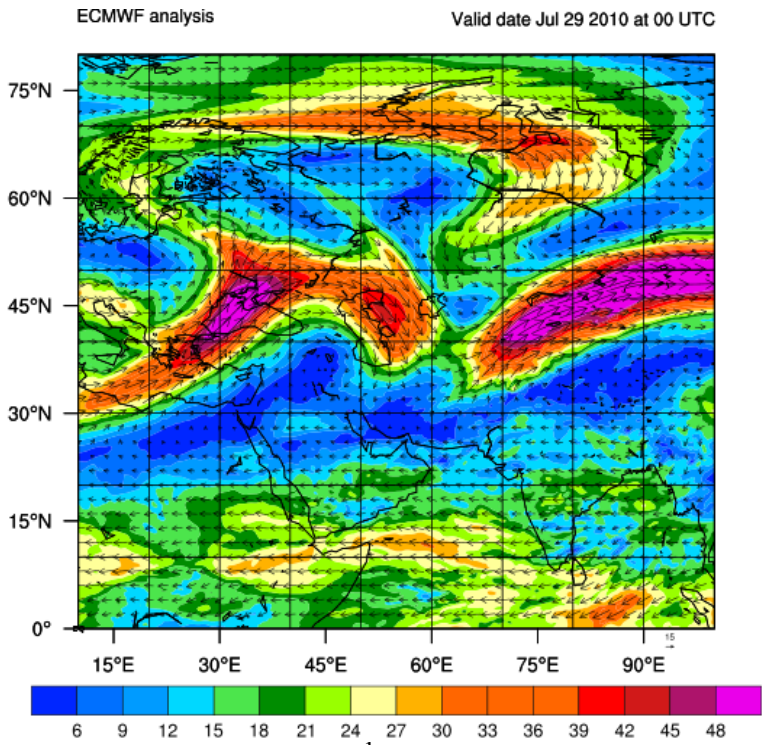

Fig. 5. Wind speed ($m\,s^{-1}$) and direction at 200 hPa for 29 July at 00:00 UTC. Data is based on ECMWF operational analysis.

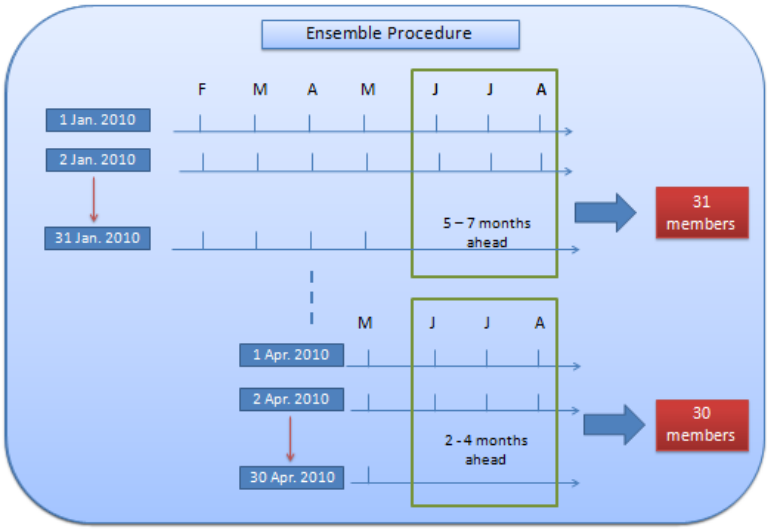

Fig. 6. Schematic representation of the seasonal simulations ensemble procedure.

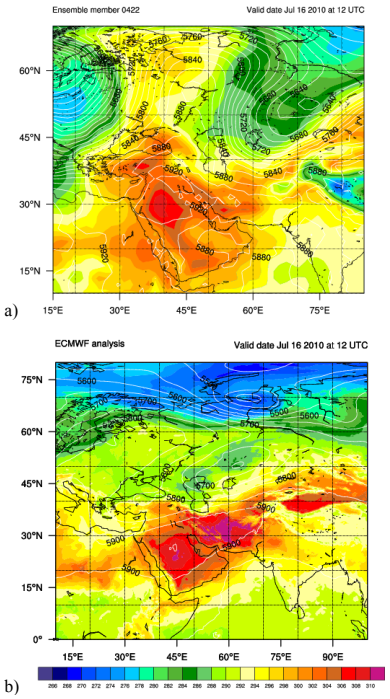

Fig. 7. Temperature at 850 hPa (˚K) and geopotential height (gpm) at 500 hPa for 16 July 2010 at 12:00 UTC based on **(a)** ensemble member initialized at 22 April 2010 and **(b)** ECMWF operational analysis.

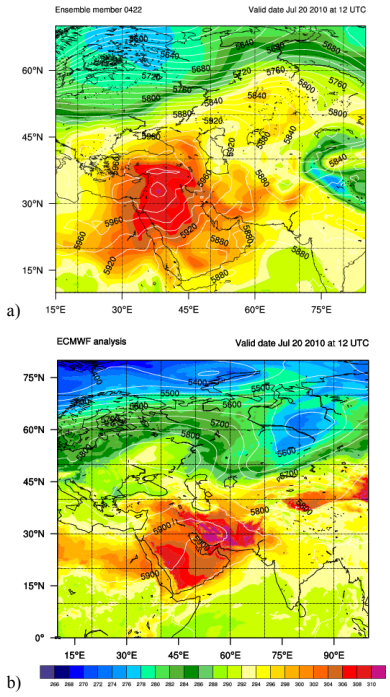

Fig. 8. Temperature at 850 hPa (˚K) and geopotential height (gpm) at 500 hPa for 20 July 2010 at 12:00 UTC based on **(a)** ensemble member initialized at 22 April 2010 and **(b)** ECMWF operational analysis.

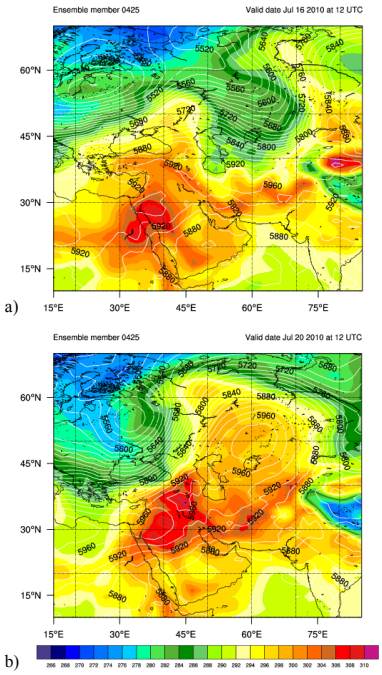

Fig. 9. Temperature at 850 hPa (°K) and geopotential height (gpm) at 500 hPa at 12:00 UTC for **(a)** 16 July 2010 and **(b)** 20 July 2010 from ensemble member initialized at 25 April 2010.

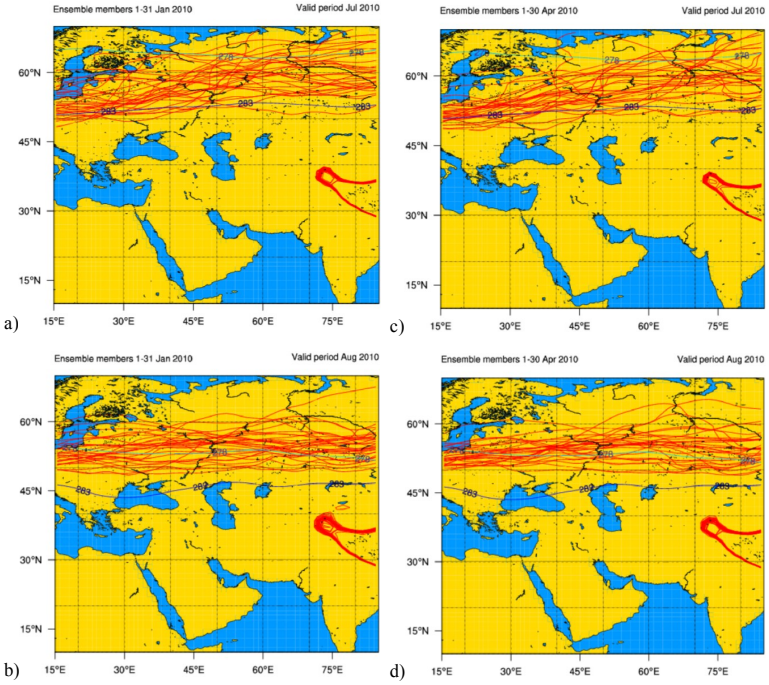

Fig. 10. Spaghetti plots (red solid lines) of the July and August 2010 mean monthly temperature at 850 hPa isotherms of 283 °K (10 °C) for the ensemble members initialized at January 2010 **(a, b)** at April 2010 **(c, d)**. NCEP long-term mean monthly isotherms at 850 hPa of 283 °K (10 °C) and 278 °K (5 °C) are denoted in blue and cyan solid lines respectively.

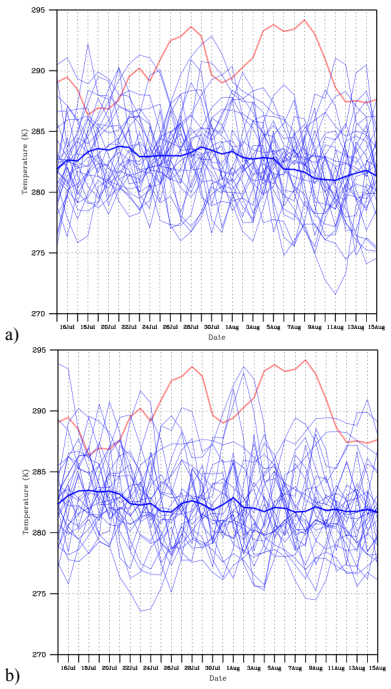

Fig. 11. Maximum daily temperatures at 850 hPa (blue thin lines) integrated over Eastern Europe and Russia of the ensemble members initialized at **(a)** January and **(b)** April valid for the period 15 July to 15 August 2010. Ensemble means are denoted with blue thick lines and the red line corresponds to the ECMWF operational analyses.

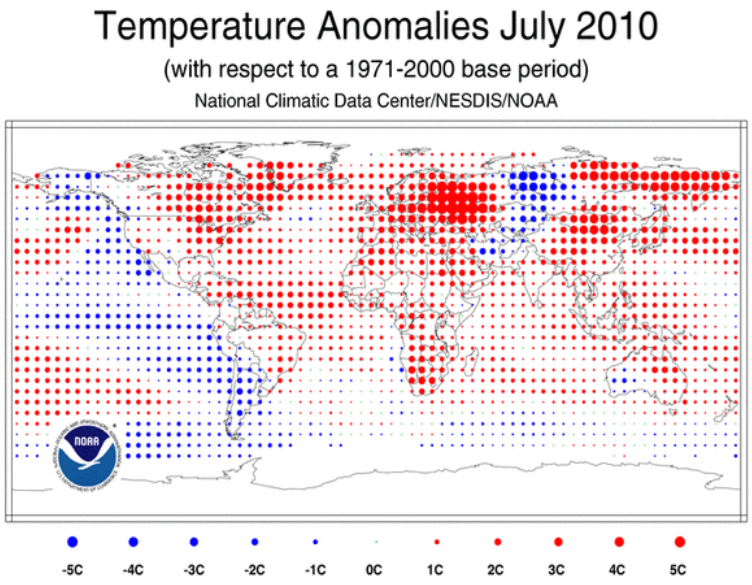

Fig. 12. Mean temperature anomalies (°C) for July 2010 with respect to 1971–2000 base period. (Source: National Climatic Data Center, NESDIS/NOAA).

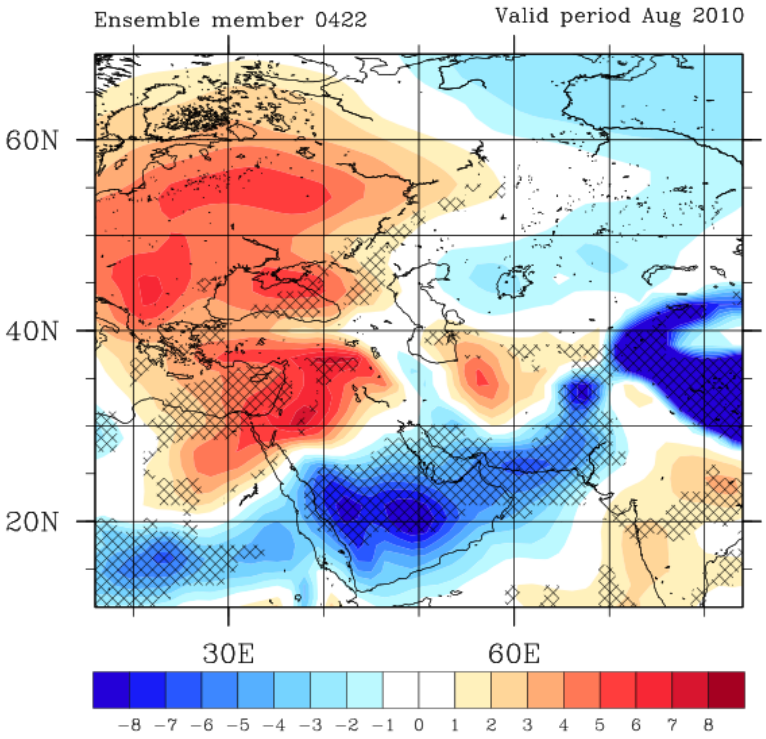

Fig. 13. Mean monthly temperature anomaly (°K) at 850 hPa for August 2010 based on the ensemble member initialized at 22 April, 00:00 UTC. Shaded areas exceed the 95 % confidence level.

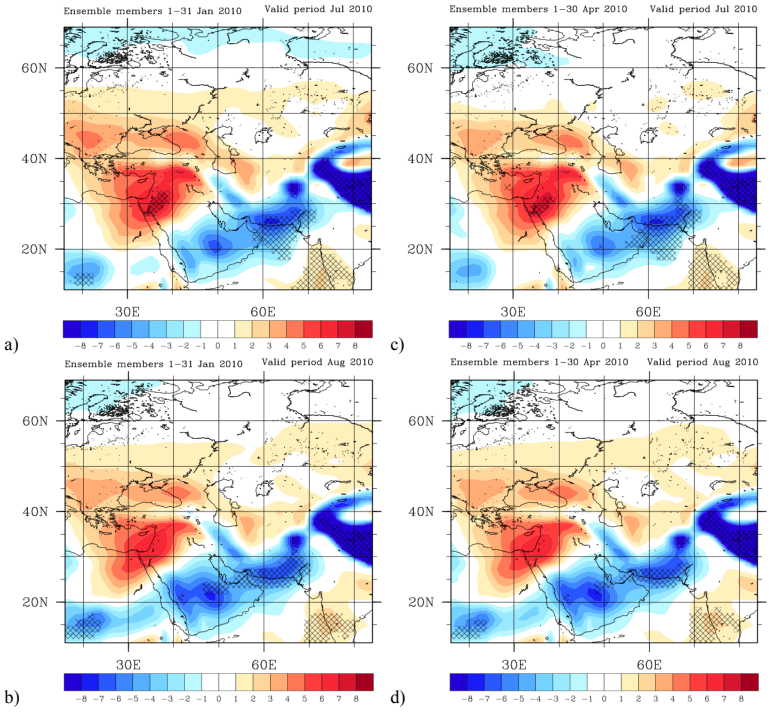

Fig. 14. Mean monthly temperature anomaly (°K) at 850 hPa for July and August 2010 based on the ensemble members initialized at January 2010 **(a, b)**, at April 2010 **(c, d)**. Shaded areas exceed the 95 % confidence level.